Frequency modulation of an aerodynamic whistle-based bat deterrent

Zhangming Zeng[a], Anupam Sharma[a]

[a]*Department of Aerospace Engineering, 537 Bissell Rd, Ames, 50011, Iowa, US*

Abstract

The aerodynamic whistle-based bat deterrent by Zeng and Sharma 2021, ("Aerodynamic-whistles-based ultrasonic tone generators for bat deterrence," *Physics of Fluids*, **35**, 2021) is numerically and experimentally analyzed for frequency modulation. Supply air pressure is modulated at various frequencies, amplitudes, and waveforms. At low frequencies (up to 100 Hz), the whistle exhibits quasi-steady behavior, and the radiated ultrasound follows the prescribed modulation. However, modulation at higher frequencies introduces multiple tones and distorts the modulation pattern. Measured farfield acoustic spectrograms reveal waveform skewness, likely due to nonlinear wave propagation in the conduit between the regulator and the whistle.

Keywords: ultrasonic whistle, frequency modulation

1. Introduction

Wind energy poses a significant anthropogenic threat to bat populations (Cryan and Brown, 2007; Cryan, 2011), and is a primary source of direct fatality for select species (O'Shea et al., 2016). Voigt et al. (2022) conducted field surveys in Germany and estimated that more than 70 bats were killed per wind turbine, or 39 per megawatt (MW) of capacity, during a two-month portion of the migration season. They emphasize that this figure is likely a conservative estimate. A recent study in Spain (Sánchez-Navarro et al., 2023) estimates the annual wind-related bat fatality rate to be 26.4 per MW. Considering the 2023 wind energy capacity in the US of approximately 147,500 MW, gives a staggering mortality rate estimate of nearly 4 million bats per year. In conjunction with existing environmental challenges such as White-nose Syndrome, wind-related bat fatality is placing certain bat species on the edge of extinction (Frick et al., 2020; Friedenberg and Frick, 2021; Cheng et al., 2021).

Operational mitigation (Baerwald et al., 2009; Arnett et al., 2013; Martin et al., 2017), which involves shutting down turbines at low wind speeds, is effective at reducing bat fatalities but it reduces energy capture. The use of deterrents to drive bats away from wind turbines is an alternative approach that minimizes/avoids power curtailment associated with operational mitigation. Bats use echolocation at ultrasonic frequencies for navigation and foraging and therefore avoid areas with high-amplitude ultrasound that interferes with their echolocation signals (Horn et al., 2008). Ultrasonic bat deterrents have shown promise in reducing wind-turbine-related bat fatalities (Weaver et al., 2020).

Schirmacher (2020) illustrated that the ultrasonic deterrence signal need not be broadband; a tonal spectrum also exhibits bat deterrence efficacy. In contrast to broadband signals, a tonal signal or spectrum concentrates its acoustic energy in specific frequencies, enhancing the intensity of these tones and enabling an extended range. Zeng and Sharma (2023) designed, prototyped, and evaluated ultrasonic bat deterrents based on the concept of aerodynamic whistles that generate a tonal spectrum via flow-acoustic resonance. These deterrents use pressurized air to excite resonance,

and are hence classified as "active". Aerodynamic whistle-based "passive" deterrents have also been explored (see e.g., Zeng et al., 2022; Sharma and Zeng, 2022), which utilize blade-relative airflow when mounted on turbine blades.

A significant challenge for ultrasonic deterrents relying on tonal noise is the capability of bats to modify the frequency of their calls (Simmons et al., 1978; Simmons and Stein, 1980; Neuweiler, 1990). Bats can potentially avoid/ignore the deterrence signal (stimulus) potentially by switching their echolocation frequency away from those of the deterrent. The frequency range over which some bat species can echolocate is as high as 50 kHz. One strategy to address this challenge is to generate a multitude of tones within the common frequency range utilized by bats. The electromechanical deterrent evaluated by Schirmacher (2020); Weaver et al. (2020) and the aerodynamic whistle-based deterrent by Zeng and Sharma (2023) produce six tones between 20 and 50 kHz; harmonics of these tones are also present in the deterrence signal. Despite having a rich tonal (or even broadband) spectrum, there is a concern that bats can get habituated to the stimulus. Evidence of such habituation has been documented in Packman et al. (2015) for *sopranos pipistrelle* bats, although Zeale et al. (2016) noted no habituation to ultrasonic deterrence for *myotis nattereri* bats over a period of 15 days. Habituation effects may therefore be species-specific in bats.

The probability of bat habituation can potentially be reduced by making the stimulus dynamic, which can be achieved by modulating the frequency and/or the amplitude of the signal. In this paper, we investigate frequency modulation of the deterrence signal of active aerodynamic whistles. The focus is on the ability of the whistles to generate dynamic signals and the modulation that can be achieved, not on bat response to the stimulus. The specific aerodynamic whistle examined in this work is the "baseline" whistle of Zeng and Sharma (2023). When supplied with a steady high-pressure air supply, the whistle generates a tonal spectrum with a peak (fundamental) frequency between $22 - 24$ kHz. Frequency modulation is achieved by temporally varying the pressure of the supply air to the deterrent.

2. Methodology

2.1. Experiments

The experiments were performed in the anechoic chamber at Iowa State University (ISU). Figure 1a shows the ultrasonic whistle mounted in the chamber and the farfield microphone arc where the radiated acoustic field was measured. As in our previous work (Zeng et al., 2022; Zeng and Sharma, 2021), the pressure signal at 30° polar angle downstream of the whistle outlet was selected to represent the radiating sound. Zeng and Sharma (2023) describes the setup and the measurement system in detail (see fig. 1); only the changes to achieve the desired modulation are discussed here. The flow control system, responsible for delivering compressed air to the whistle, was modified as follows. An ENFIELD Technologies LS-V15s high-speed proportional directional valve was added (fig. 1b) to modulate the supply pressure of the air entering the whistle; we refer to it as a pressure regulator. An OMEGA PX309-015G5V pressure transducer was installed immediately upstream of the whistle to monitor the static pressure of the airflow (fig. 1a). Since the flow speed of supply air is sufficiently low, the difference between static and total pressure is neglected. Therefore, the static pressure measured by the transducer is treated as the total pressure (p_0) of the air supplied to the whistle. The time-varying total pressure, $p_0(t)$ is expressed as

$$p_0(t) = \bar{p}_0 + p_0'(t), \tag{1}$$

where $\bar{p}_0$ represents the time-averaged value, and $p_0'(t)$ denotes the prescribed perturbation pressure. Periodic variations in time for $p_0'(t)$ are considered with sine, square, and triangle waveforms; the

modulation frequency and amplitude are denoted by f_m and p_m respectively. The primary waveform investigated is the sine wave for which $p_0'(t) = p_m \sin(2\pi f_m t)$.

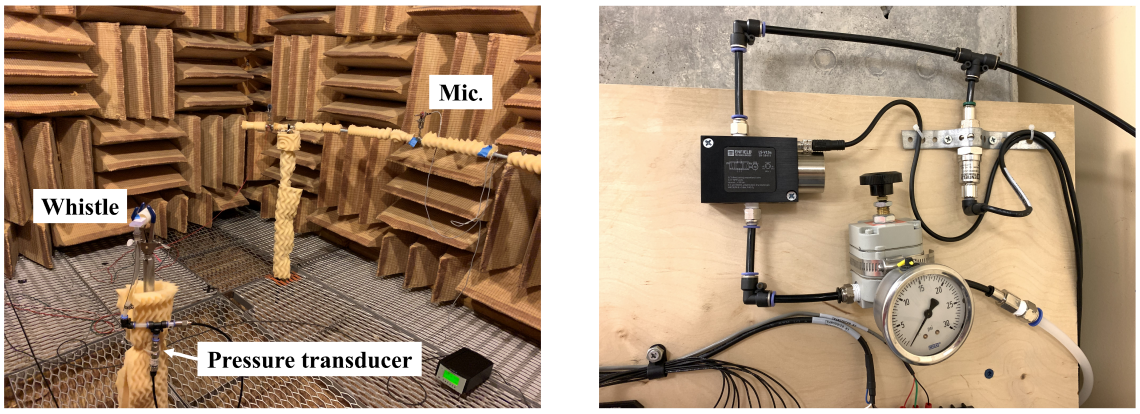

(a) setup in the anechoic chamber

(b) equipment to modulate supply pressure

Figure 1: Experimental setup for investigating the effect of modulating supply air pressure on radiated sound from the baseline ultrasonic whistle of Zeng and Sharma (2023). (a) the whistle, microphone, and pressure transducer installed in the Iowa State anechoic chamber, and (b) equipment to modulate the supply air pressure.

2.2. Numerical Simulations

Two-dimensional computational fluid dynamics (2D CFD) simulations are performed to complement the experiments and investigate the effect of inflow pressure modulation. The flow field is computed by solving the unsteady Reynolds-averaged Navier-Stokes (uRANS) equations. The computational domain, mesh, and the numerical model used in this work are the same as those in Zeng and Sharma (2023); the inlet boundary condition is modified to time-varying total pressure, $p_0(t)$. Figure 2a shows the instantaneous pressure contours of the radiating acoustic field from one of the simulations. Data probes are placed inside the computational domain, including at the center of each chamber (fig. 2b) to gather time-resolved pressure data.

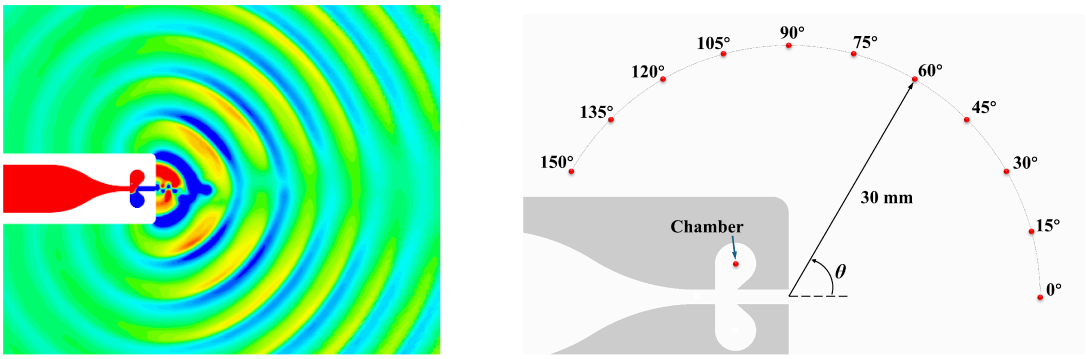

(a) instantaneous pressure contours

(b) probe locations

Figure 2: Two-dimensional computational fluid dynamics analysis. (a) A visualization of the radiating acoustic waves using instantaneous pressure contours, and (b) locations where time-accurate data is collected for spectral analysis.

3. Results

Table 1 lists the different cases investigated. They span a range of frequencies (f_m), amplitudes (p_m), and types of waveform (sine, square, and triangle) used to modulate the supply pressure.

Table 1: A list/values of parameters explored. The mean supply pressure, $\bar{p}_0 = 2$ psig for all cases.

f_m (Hz)	p_m (psi)	*Waveform*
10	1	sine, triangle, square
50	1,2	sine
100	1	sine, triangle, square
100	2	sine
400	1	sine
1000	1	sine

3.1. Numerical Results

We first illustrate the typical behavior of the whistle by analyzing the numerical results for one of the cases where the inlet total pressure is prescribed as follows: $f_m = 50$ Hz, $p_m = 1.0$ psi, and sine waveform. Figure 3 plots the spectrograms of pressure inside one of the resonating chambers of the whistle (left panel) and the radiated farfield acoustics (right panel). The primary peak in the chamber is around 12 kHz while in the farfield it is approximately 24 kHz. This is due to the out-of-phase operation of the two chambers, canceling the odd harmonics ($\approx$ 12 and 36 kHz) and radiating only the even harmonics ($\approx$ 24 and 48 kHz) from the whistle. The result is expected based on our analysis of the whistle for steady inlet supply pressures (see Zeng and Sharma, 2023). With a sinusoidal inlet total pressure variation, a nearly sinusoidal modulation of the peak frequencies of the radiated sound is observed for this case.

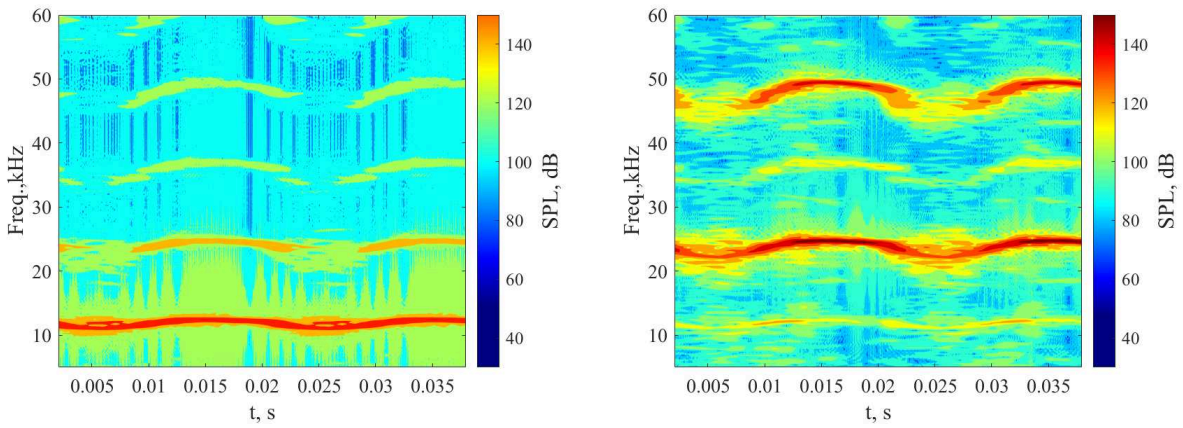

(a) At the center of a chamber

(b) In the farfield at 30° polar angle

Figure 3: Spectrograms of numerically simulated pressure for the case with $f_m = 50$ Hz, $p_m = 1.0$ psi, sine waveform. (a) At the center of one of the resonating chambers, and (b) at a farfield point at 30° polar angle.

To quantitatively assess the frequency modulation, the peak frequencies from the pressure spectrograms are extracted and plotted over two cycles in fig. 4. The peak frequencies at the chamber center and in the farfield oscillate with the modulation frequency (f_m) of the inlet total pressure ($p_0(t)$); the phase on the abscissa of fig. 4 is of $p_0(t)$. The nearly sinusoidal modulation of the peak frequency, reproducing the modulation in $p_0(t)$, suggests that the process is quasi-steady for this case. A semi-transparent band around the peak frequency is added to account for the spreading of energy into adjacent frequencies. The limits of the frequency band are determined by the radiated sound pressure level (SPL) falling 10 dB below the peak value.

The effect of varying f_m on the radiating acoustic spectra is assessed numerically. f_m is varied

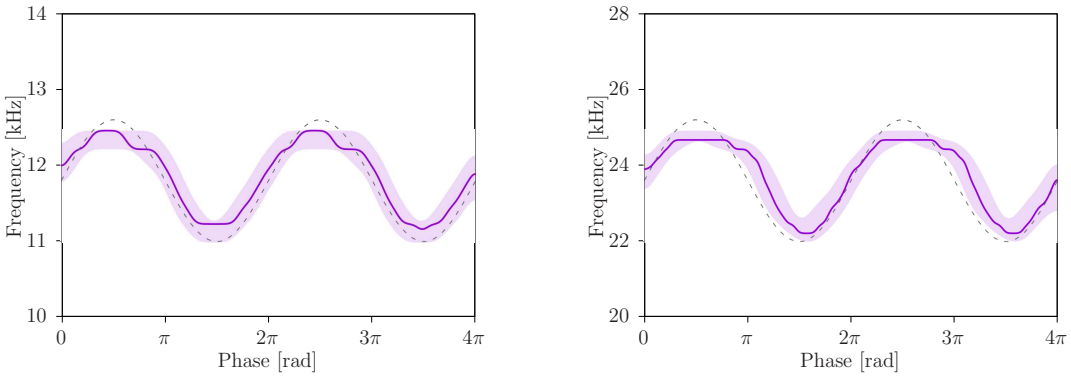

(a) At the center of a chamber

(b) In the farfield at 30° polar angle

Figure 4: Variation of peak frequencies (a) at the center of a resonating chamber, and (b) in the farfield at 30° polar angle. The semitransparent region shows the frequency range where the SPL is within 10 dB of the peak SPL value. The abscissa shows the phase of the supply pressure, $p_0(t)$, which is modulated with $f_m = 50$ Hz, $p_m = 1$ psi, sine waveform; the gray dashed line shows the qualitative variation of $p_0(t)$ for reference.

from 50 to 1000 Hz while keeping p_m fixed at 1 psi; the spectrograms are plotted in fig. 5 for four values of f_m. For small f_m (50, 100 Hz), the modulation can be treated as a quasi-steady process. The separation of time scales between the signal ($f_m \sim 100$ Hz) and the radiating acoustics (peak $f \sim 23$ kHz) is very large, and hence the whistle nearly reaches an equilibrium before any measurable change in inlet pressure occurs. Therefore, the radiated acoustic spectrum is modulated similarly to the supply pressure. The peak frequency increases with supply pressure, as observed in our steady analysis (see Zeng and Sharma, 2023).

As f_m increases to 400 Hz (panel c in fig. 5), nonlinear behavior, characterized by the presence of multiple tones around the peak frequency, is observed. The multiple tones around each peak frequency are contained in a frequency band that remains nearly time-invariant; a hint of frequency modulation is observed but it is not at f_m. As f_m increases to 1000 Hz, the frequency bands widen.

Variations of peak frequency with the phase of inlet total pressure are plotted in fig. 6a for $f_m = 50$ and 100 Hz. Due to the presence of multiple frequencies of similar magnitudes, it is difficult to determine a precise peak frequency for higher f_m. The quasi-steady behavior for low f_m ($= 50, 100$ Hz) is apparent in the plot; the curves show a near-sinusoidal behavior. The highest frequency achieved in the radiating field does not vary with f_m, however, the lowest frequency increases with f_m; the modulated frequency range therefore reduces with increasing f_m. The larger the separation of time scales, the more quasi-steady the process, and the higher the modulated frequency range. Figure 6b shows that the trend with varying f_m remains the same when p_m is increased from 1 to 2 psi.

Figure 7 illustrates the effect of varying p_m. Increasing p_m increases the mean value about which the peak frequency modulates; this increase/shift is more apparent for $f_m = 100$ Hz (fig. 7b) Three different waveforms – sine, square, and triangle – of the modulating signal are evaluated for $f_m = 100$ Hz and $p_m = 1$ psi (fig. 8). The difference between triangle and sine waveforms is negligible, but the square wave shows a perceptible difference. Altering the waveform has little to no effect on the highest and lowest values of the radiated peak frequency.

3.2. Experimental Results

Experiments were conducted in the ISU anechoic chamber to complement the numerical findings. Figure 9a illustrates a typical measurement result showing the farfield sound spectrogram for the

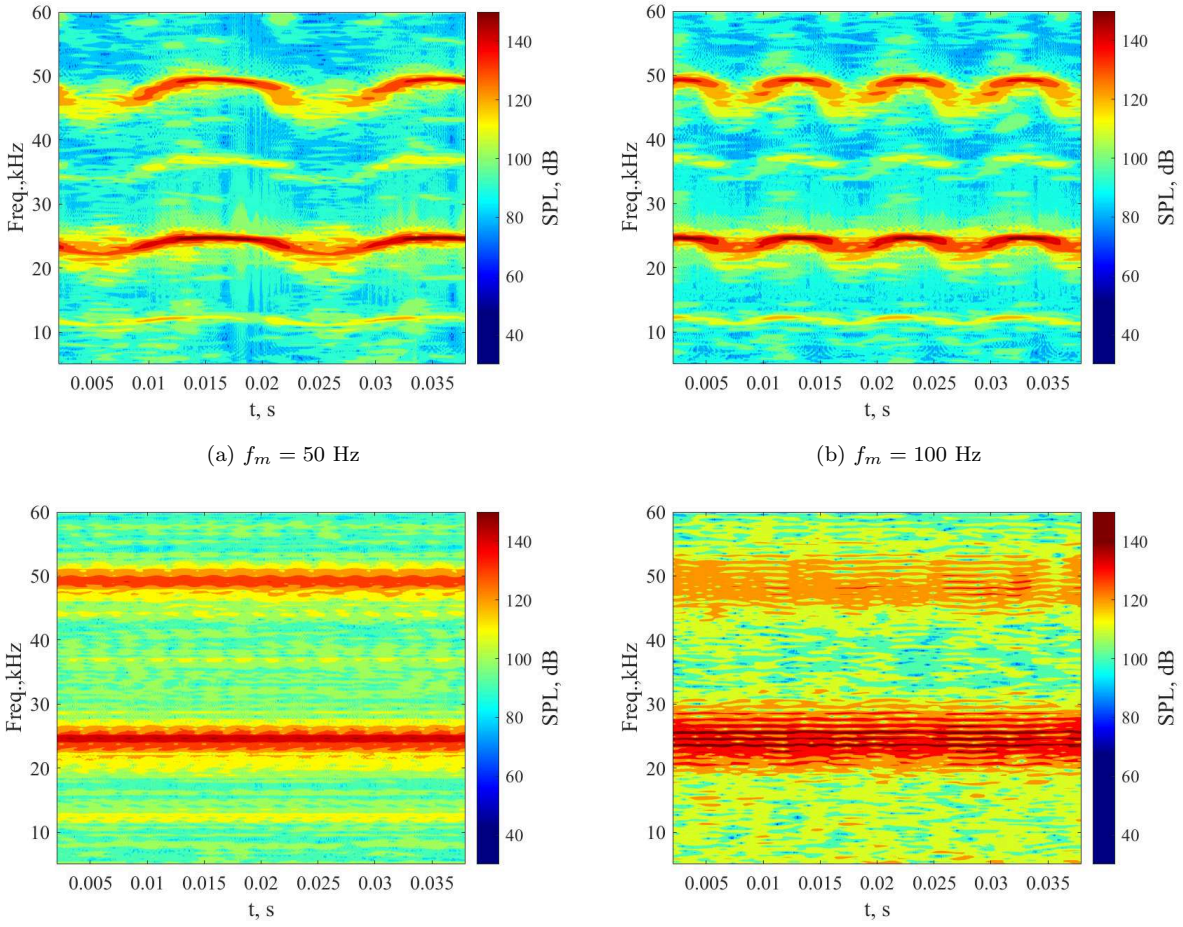

(a) $f_m = 50$ Hz

(b) $f_m = 100$ Hz

(c) $f_m = 400$ Hz

(d) $f_m = 1000$ Hz

Figure 5: CFD spectrograms depicting the radiating noise at various f_m ($p_m = 1.0$ psi).

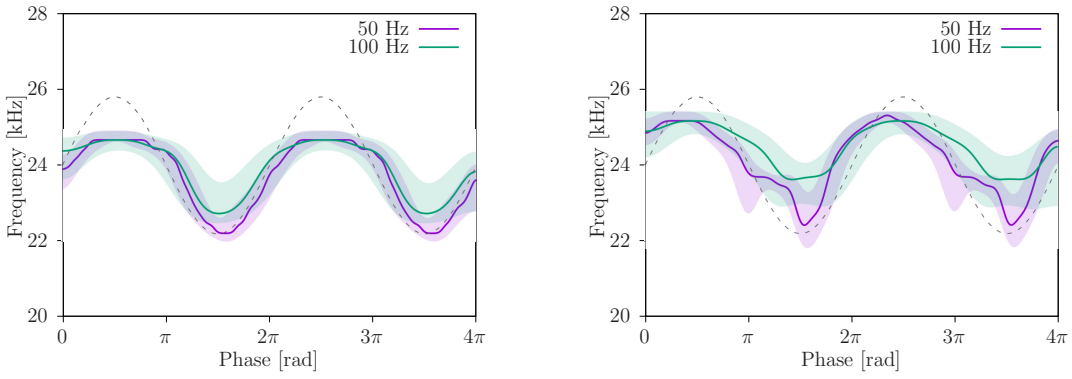

(a) $p_m = 1$ psi

(b) $p_m = 2$ psi

Figure 6: Peak frequency-phase relationships for sinusoidal modulation of inlet pressure for two values of f_m (= 50, 100 Hz) for (a) $p_m = 1$ psi, and (b) $p_m = 2$ psi.

following parameters: $f_m = 50$ Hz, $p_m = 1.0$ psi, and sine waveform. Frequency modulation is observed in the measurements, however, the waveform is skewed.

The skewness in the experimental data (fig. 9) is due to nonlinear wave propagation in the pipe

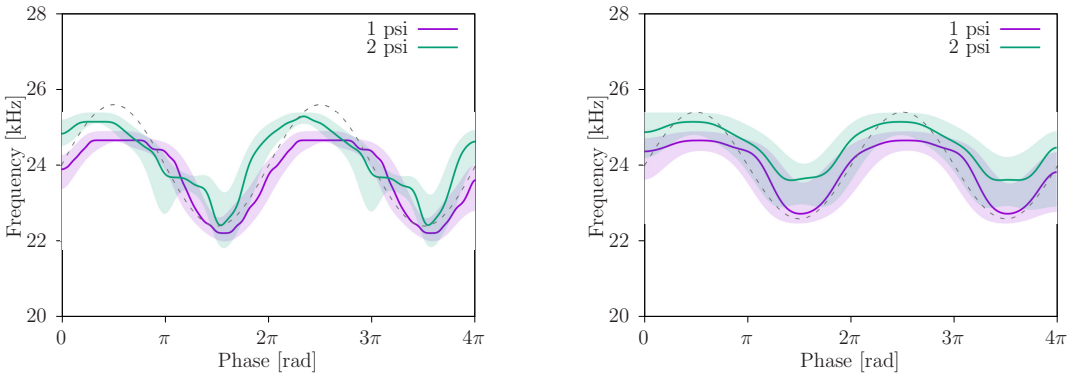

(a) $f_m = 50$ Hz (b) $f_m = 100$ Hz

Figure 7: Peak frequency-phase relationships for two values of p_m (=1, 2 psi). The modulating signal waveform is a sine wave.

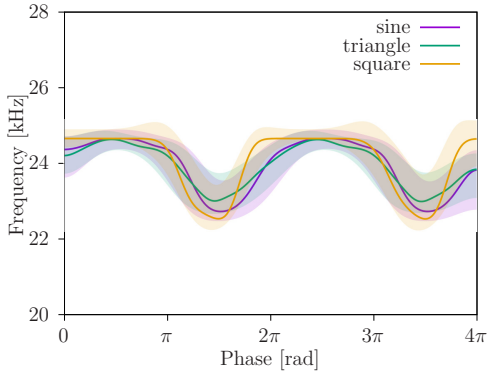

Figure 8: Peak frequency-phase relationships for three waveforms of the modulating signal – sine, square, and triangle; $f_m = 100$ Hz and $p_m = 1.0$ psi.

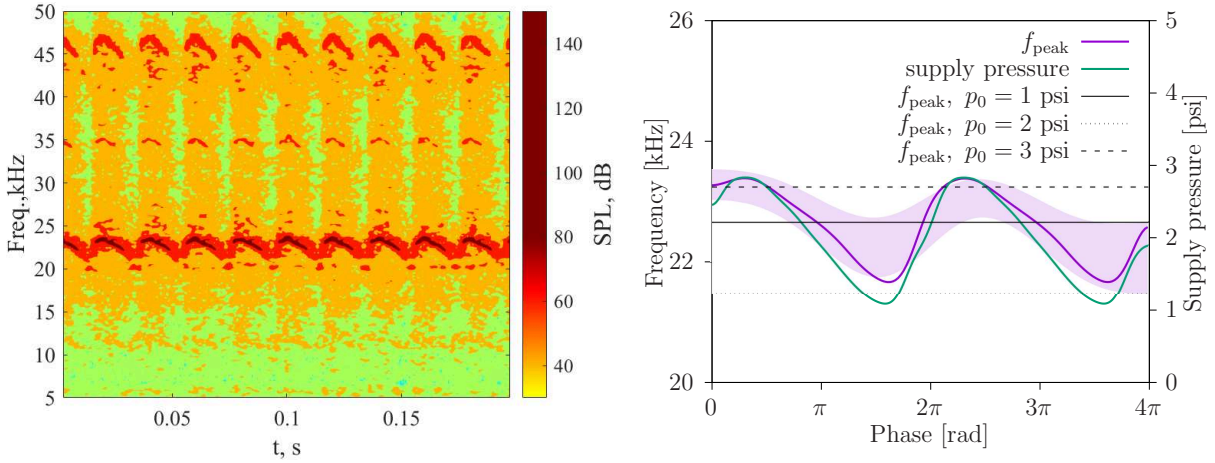

(a) Farfield pressure spectrogram (b) f_{peak} and supply pressure variation

Figure 9: Experimental results for $f_m = 50$ Hz, $p_m = 1.0$ psi, sine-wave modulation. (a) Measured farfield pressure spectrogram, and (b) variation of peak frequency and supply pressure at whistle inlet with phase; the dotted, solid, and dashed black lines refer to the peak frequencies for steady cases with $p_0 = 1,\ 2$, and 3 psi respectively.

from the pressure regulator to the whistle inlet (see appendix Appendix A). The supply pressure, measured immediately upstream of the whistle also shows similar skewness as the peak radiated frequency (fig. 9b). In the numerical simulations, pressure modulation is applied directly at whistle inlet and hence wave steepening is not present.

The dominant frequencies for steady air supply to the whistle at pressures of $1, 2$ and 3 psig are also identified in fig. 9b. The highest and lowest frequencies in the measurement with modulating air supply align with the static results for $p_0 = 1$ and 3 psig respectively. This supports the hypothesis that at low f_m, the modulation of the radiated acoustics can be approximated as quasi-steady. The phase-averaged peak frequency-phase relationships for different f_m are plotted in fig. 10. As f_m increases, nonlinear dissipation during wave propagation increases and frequency modulation is reduced. The effect of modulation waveform is examined in fig. 11. Wave steepening nearly eliminates the differences between the sine and triangle waveforms at $f_m = 10$ Hz. At higher f_m (=100 Hz), nonlinear dissipation reduces the pressure variation seen by the whistle and all three waveforms are nearly identical.

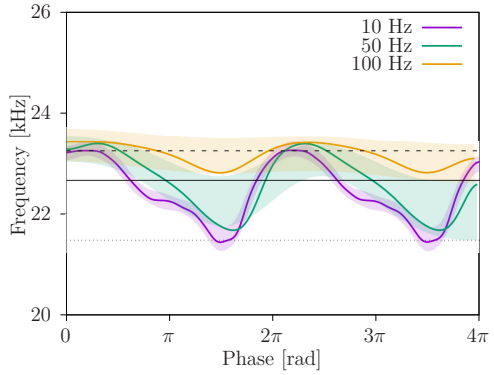

Figure 10: Phase-averaged peak frequency oscillation per cycle of measured radiated noise for three values of f_m under $p_m = 1$ psi, sine-wave modulation.

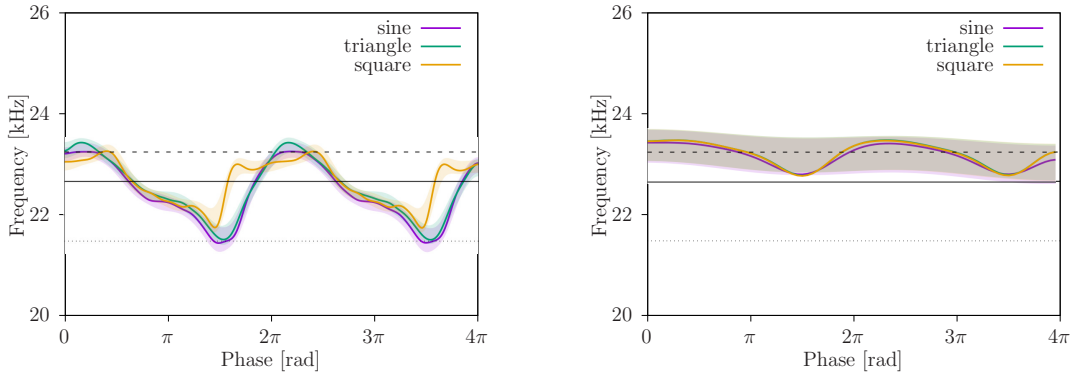

(a) $f_m = 10$ Hz

(b) $f_m = 100$ Hz

Figure 11: Peak frequency-phase relationships for sine, square, and triangular waveforms. (a)$f_m = 10$ Hz and (b)$f_m = 100$ Hz; $p_m = 1$ here.

4. Conclusion

Frequency modulation of the aerodynamic ultrasonic whistle by Zeng and Sharma (2023) is examined numerically and experimentally. Modulation is achieved by temporally varying the supply pressure. The influence of the frequency (f_m), amplitude (p_m), and waveform of supply pressure are evaluated. At low f_m, the modulation is quasi-steady, with the whistle reaching equilibrium before any measurable change in supply pressure occurs. As f_m is increased (from 100 to 1000 Hz), multiple tones appear around the peak frequency and the prescribed frequency modulation is not observed in the radiated sound spectrograms. Frequency modulation (at low f_m) is confirmed in the experiments. Nonlinear wave propagation in the pipe between the regulator and the whistle leads to skewness (wave steepening) in the waveform and a reduction (nonlinear dissipation) in the amplitude of radiated frequency modulation. In summary, this research confirms that varying the supply pressure of the active deterrent can be effectively used to modulate the frequency of the stimulus, which may reduce the possibility of bat habituation.

Acknowledgments

This work was supported by the U.S. Department of Energy's Office of Energy Efficiency and Renewable Energy (EERE) under the Wind Energy Technologies Office Award Number DE-EE0008731 and DE-EE0011086. The National Science Foundation (Grants CBET-1554196 and 1935255) also partially supported this research. We also acknowledge the computational resources provided by the Department of Defense through the US Air Force Office of Scientific Research (Award # FA9550-23-1-0016) and the Iowa State University.

Credits

Conceptualization: AS; **Data curation:** ZZ; **Formal analysis:** ZZ; **Funding acquisition:** AS; **Investigation:** AS, ZZ; **Methodology:** AS, ZZ; **Project administration:** AS; **Resources:** AS; **Software:** ZZ; **Supervision:** AS; **Validation:** ZZ; **Visualization:** AS, ZZ; **Writing – original draft:** ZZ; **Writing – review & editing:** AS

Appendix A. Wave propagation in the supply pipe

Pressure is measured at two points in the supply pipe – one immediately downstream of the pressure regulator and one immediately upstream of the whistle. Figure A.12 compares the waveforms of pressure at the two locations; a sinusoidal pressure waveform is imposed by the regulator. In addition to loss in overall total pressure (entire waveform shifting down), nonlinear propagation effects - reduction in peak-to-peak variation (due to nonlinear dissipation) and increased skewness in waveform (due to wave steepening) are observed.

References

Arnett, E.B., Hein, C.D., Schirmacher, M.R., Huso, M.M., Szewczak, J.M., 2013. Evaluating the effectiveness of an ultrasonic acoustic deterrent for reducing bat fatalities at wind turbines. PloS one 8.

Baerwald, E.F., Edworthy, J., Holder, M., Barclay, R.M., 2009. A large-scale mitigation experiment to reduce bat fatalities at wind energy facilities. The Journal of Wildlife Management 73, 1077–1081.

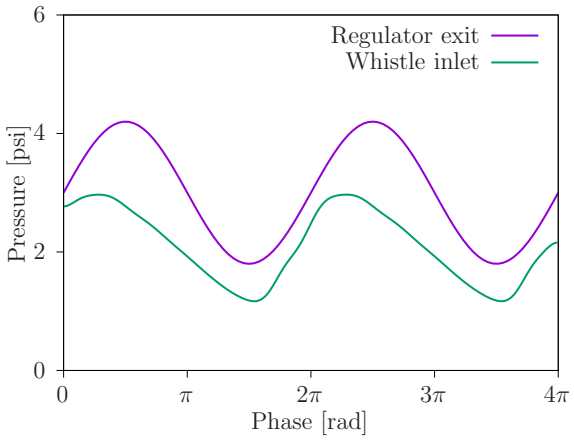

Figure A.12: Pressure waveforms at different locations in the supply pipe. A sinusoidal variation in pressure is introduced by the regulator. Nonlinear propagation leads to reduction in peak-to-peak variation and increased skewness while friction cause the overall pressure drop.

Cheng, T.L., Reichard, J.D., Coleman, J.T., Weller, T.J., Thogmartin, W.E., Reichert, B.E., Bennett, A.B., Broders, H.G., Campbell, J., Etchison, K., et al., 2021. The scope and severity of white-nose syndrome on hibernating bats in north america. Conservation Biology 35, 1586–1597.

Cryan, P.M., 2011. Wind turbines as landscape impediments to the migratory connectivity of bats. Environmental Law , 355–370.

Cryan, P.M., Brown, A.C., 2007. Migration of bats past a remote island offers clues toward the problem of bat fatalities at wind turbines. Biological conservation 139, 1–11.

Frick, W.F., Kingston, T., Flanders, J., 2020. A review of the major threats and challenges to global bat conservation. Annals of the New York Academy of Sciences 1469, 5–25.

Friedenberg, N.A., Frick, W.F., 2021. Assessing fatality minimization for hoary bats amid continued wind energy development. Biological Conservation 262, 109309.

Horn, J.W., Arnett, E.B., Jensen, M., Kunz, T.H., 2008. Testing the effectiveness of an experimental acoustic bat deterrent at the maple ridge wind farm. Report Prepared for: The Bats and Wind Energy Cooperative and Bat Conservation International, Austin, TX .

Martin, C.M., Arnett, E.B., Stevens, R.D., Wallace, M.C., 2017. Reducing bat fatalities at wind facilities while improving the economic efficiency of operational mitigation. Journal of Mammalogy 98, 378–385.

Neuweiler, G., 1990. Auditory adaptations for prey capture in echolocating bats. Physiological reviews 70, 615–641.

O'Shea, T.J., Cryan, P.M., Hayman, D.T., Plowright, R.K., Streicker, D.G., 2016. Multiple mortality events in bats: a global review. Mammal review 46, 175–190.

Packman, C., Zeale, M., Harris, S., Jones, G., 2015. Management of Bats in Churches - a pilot. Technical Report. University of Bristol.

Sánchez-Navarro, S., Gálvez-Ruiz, D., Rydell, J., Ibáñez, C., 2023. High bat fatality rates estimated at wind farms in southern spain. Acta Chiropterologica 25, 125–134.

Schirmacher, M.R., 2020. Evaluating the effectiveness of an ultrasonic acoustic deterrent in reducing bat fatalities at wind energy facilities. Technical Report. Bat Conservation International, Austin, TX (United States).

Sharma, A., Zeng, Z., 2022. Passive Ultrasonic Deterrents to Reduce Bat Mortality in Wind Farms. Technical Report DE-EE0008731. Department of Energy.

Simmons, J.A., Lavender, W., Lavender, B., Childs, J., Hulebak, K., Rigden, M., Sherman, J., Woolman, B., O'Farrell, M.J., 1978. Echolocation by free-tailed bats (tadarida). Journal of Comparative Physiology 125, 291–299.

Simmons, J.A., Stein, R.A., 1980. Acoustic imaging in bat sonar: echolocation signals and the evolution of echolocation. Journal of comparative physiology 135, 61–84.

Voigt, C.C., Kaiser, K., Look, S., Scharnweber, K., Scholz, C., 2022. Wind turbines without curtailment produce large numbers of bat fatalities throughout their lifetime: A call against ignorance and neglect. Global Ecology and Conservation 37, e02149.

Weaver, S.P., Hein, C.D., Simpson, T.R., Evans, J.W., Castro-Arellano, I., 2020. Ultrasonic acoustic deterrents significantly reduce bat fatalities at wind turbines. Global Ecology and Conservation 24, e01099.

Zeale, M.R., Bennitt, E., Newson, S.E., Packman, C., Browne, W.J., Harris, S., Jones, G., Stone, E., 2016. Mitigating the impact of bats in historic churches: the response of natterer's bats myotis nattereri to artificial roosts and deterrence. PLoS One 11, e0146782.

Zeng, Z., Sharma, A., 2021. Experimental and numerical aeroacoustic analysis of an ultrasound whistle, in: AIAA Aviation Forum, Washington DC, USA.

Zeng, Z., Sharma, A., 2023. Aerodynamic-whistles-based ultrasonic tone generators for bat deterrence. Physics of Fluids 35.

Zeng, Z., Sharma, A., S-F., H., Alexander, W.N., 2022. Passive operation of a blade-mounted, ultrasonic bat deterrent using an exhaust diffuser, in: 28th AIAA/CEAS Aeroacoustics 2022 Conference, p. 3101.